JVI Accepted Manuscript Posted Online 18 July 2018
J. Virol. doi:10.1128/JVI.00683-18

1 **Middle East respiratory syndrome coronavirus spike protein is not activated**
2 **directly by cellular furin during viral entry into target cells**
3

4 Shutoku Matsuyama,[a#] Kazuya Shirato,[a] Miyuki Kawase,[a] Yutaka Terada,[c] Kengo
5 Kawachi,[c] Shuetsu Fukushi,[b] and Wataru Kamitani[c]
6
7 [a]Department of Virology III, National Institute of Infectious Diseases, Tokyo, Japan
8 [b]Department of Virology I, National Institute of Infectious Diseases, Tokyo, Japan
9 [c]Laboratory of Clinical Research on Infectious Diseases, Osaka University, Osaka, Japan
10
11 **Running Head:** Cell entry by MERS-CoV is not dependent on furin
12
13 #Address correspondence to Shutoku Matsuyama, matuyama@nih.go.jp.
14

ABSTRACT

Middle East respiratory syndrome coronavirus (MERS-CoV) utilizes host cellular proteases to enter cells. A previous report shows that furin, which is distributed mainly in the Golgi apparatus and cycled to the cell surface and endosomes, proteolytically activates the MERS-CoV spike (S) protein following receptor binding to mediate fusion between the viral and cellular membranes. Here, we re-examined furin usage by MERS-CoV using a real-time PCR-based virus cell entry assay after inhibition of cellular proteases. We found that the furin inhibitor dec-RVKR-CMK blocked entry of MERS-CoV harboring an S protein lacking furin cleavage sites; it even blocked entry into furin-deficient LoVo cells. In addition, dec-RVKR-CMK not only inhibited the enzymatic activity of furin but also that of cathepsin L, cathepsin B, trypsin, papain, and TMPRSS2. Furthermore, a virus cell entry assay and a cell-cell fusion assay provided no evidence that the S protein was activated by exogenous furin. Therefore, we conclude that furin does not play a role in entry of MERS-CoV into cells, and that the inhibitory effect of dec-RVKR-CMK is specific for TMPRSS2 and cathepsin L rather than furin.

IMPORTANCE

Previous studies using the furin inhibitor dec-RVKR-CMK suggest that MERS-CoV utilizes a cellular protease, furin, to activate viral glycoproteins during cell entry. However, we found that dec-RVKR-CMK inhibits not only furin but also other proteases. Furthermore, we found no evidence that MERS-CoV uses furin. These findings suggest that previous studies in the virology field based on dec-RVKR-CMK should be re-examined carefully. Here, we describe appropriate experiments that can be used to assess the effect of protease inhibitors on virus cell entry.

INTRODUCTION

Many species of enveloped virus utilize host cellular proteases to infect cells (1). Two major mechanisms are responsible for proteolytic activation of viral spike (S) glycoproteins. In the case of human immunodeficiency virus and highly pathogenic avian influenza viruses, a cellular protease called furin cleaves the viral glycoprotein during biogenesis, thereby converting the precursor glycoprotein to its fusion-competent state (1–3). Alternatively, the S protein of viruses such as severe acute respiratory syndrome coronavirus (SARS-CoV) and Middle East respiratory syndrome coronavirus (MERS-CoV) is cleaved by cell surface or endosomal proteases such as transmembrane protease serine 2 (TMPRSS2), HAT, furin, trypsin, elastase, or cathepsin L. This cleavage triggers conformational changes during viral entry after the receptor-binding step (2–14). In the presence of extracellular or cell surface proteases such as elastase or TMPRSS2, MERS-CoV enters cells after binding to the cell surface receptor; however, in their absence, MERS-CoV utilizes cathepsin L in the late endosome (10). Cleavage releases the receptor-binding S1 subunit from the membrane fusion S2 subunit, which triggers conformational changes in the S2 subunit to induce membrane fusion (2).

The role of furin in activating the MERS-CoV S protein is controversial. Furin is a proprotein convertase responsible for maturation of a huge number of inactive proteins; it is localized principally in the trans-Golgi network, from where it is cycled to the cell surface and the endosomes, which are organelles used by MERS-CoV for cell entry (11). Of the furin inhibitors reported previously (15–17), dec-RVKR-CMK and a proprotein convertase inhibitor (PCI) are often used in virology experiments. Gierer et al. used a PCI to show that enzymatic processing during biogenesis of the MERS-CoV S protein by proprotein convertases such as furin is not required for infectivity; however, they stated that the host cell protease is required for S protein activation during viral uptake into target cells (14). By contrast, Park et al. used dec-RVKR-CMK to show that mutated

MERS-CoV (in which the furin cleavage site was masked) tended to enter cells via the endosomal pathway, while the wild-type (wt) virus entered at the cell via cell surface proteases; this indicates that cleavage of the S protein during biogenesis determines the tropism of the virus for different cell types (8). Furthermore, Millet and Whittaker reported that the MERS-CoV S protein harbors furin cleavage sequences at the S1/S2 and S2' sites; these sites could be targeted by host cellular furin during cell entry. Indeed, non-cytotoxic concentrations (2.5–100 μM) of dec-RVKR-CMK prevented entry of pseudotyped and authentic MERS-CoV (13). Burkard et al. used dec-RVKR-CMK to show that murine coronavirus mouse hepatitis virus (MHV) also uses furin for viral cell entry (12). However, furin is thought to make only a minor contribution to viral cell entry because MERS-CoV entry into some cell lines (even furin-expressing cells) is almost completely blocked by simultaneous treatment with a TMPRSS2 inhibitor (camostat mesylate) and a cathepsin inhibitor (E64d) (10). Here, we re-examined the role of furin during MERS-CoV infection to clarify when and how it is involved in virus cell entry. The findings question our current understanding of host protease usage underlying MERS-CoV infection.

RESULTS

Evaluation of an appropriate assay to monitor virus cell entry

First, we examined cell entry by three types of virus: 1) a pseudotyped vesicular stomatitis virus (VSV) bearing a MERS-CoV S protein in which the VSV-G gene was replaced by the green fluorescent protein (GFP) gene (VSV-ΔG/GFP-MERS-S); 2) the same virus in which the GFP gene was replaced by the luciferase (Luc) gene (VSV-ΔG/Luc-MERS-S); and 3) authentic MERS-CoV. These viruses were used to infect Vero/TMPRSS2 cells (18), which are highly susceptible to MERS-CoV (10). Entry of these viruses into cells was measured using appropriate assays (see Materials and methods). The range for VSV-ΔG/GFP-MERS-S was narrow (1–3 log10 GFP-cell

counts) (Fig. 1A), whereas that for luciferase was broad (1–5 log10 Luc unit) (Fig. 1B); however, the range for authentic MERS-CoV (assessed by real-time PCR) was broader still (2–7 log10 copies of viral mRNA) (Fig. 1C).

To evaluate the suitability of the assays for the furin inhibition experiments, we examined the effect of a furin inhibitor (dec-RVKR-CMK; 100 μM) on viral entry into cells. Infection with VSV-ΔG/GFP-MERS-S in the presence of dec-RVKR-CMK led to a fall in the number of GFP-positive cells by 60% (0.38 log) (Fig. 1D). Infection by VSV-ΔG/Luc-MERS-S in the presence of the inhibitor led to a fall of 40% (0.21 log) (Fig. 1E, left panel). By contrast, infection by authentic MERS-CoV led to a 97% (1.53 log) reduction in the viral mRNA copy number (Fig. 1F). The pseudotyped virus encoding GFP is suitable for measuring the percentage value of infection whithin a narrow range. However, we surmised that VSV-ΔG/Luc-MERS-S would not provide reliable results because the 40% reduction observed in the assay is negligible on a logarithmic scale (Fig. 1E, right panel), we must consider the quantifiable range for this virus was 4 logs, and the luminometer used in the assay has a dynamic range of 9 logs. Therefore, we used authentic MERS-CoV for experiments designed to measure the inhibitory effects of dec-RVKR-CMK.

Entry of MERS-CoV into Calu-3 cells in the presence of a furin inhibitor

To examine the effect of cellular furin on MERS-CoV infection, we infected Calu-3 cells (which are derived from human bronchial epithelial cells) with the authentic MERS-CoV in the presence of inhibitors. After a 6 h incubation at 37°C, cellular RNA was isolated and real-time PCR was carried out to quantify the amount of viral mRNA. As shown in Figure 2, a TMPRSS2 inhibitor (camostat mesylate; 10 μM) suppressed virus entry by 100-fold; similar results were observed after treatment with 20 μM dec-RVKR-CMK. E64d had little effect on virus entry, suggesting that MERS-CoV mainly uses the

TMPRSS2/cell surface pathway rather than the cathepsin/endosome pathway to enter Calu-3 cells. Taken together, the results suggest that either furin is essential for S protein activation or that dec-RVKR-CMK suppresses both furin and TMPRSS2.

Susceptibility of furin-deficient LoVo cells to infection by MERS-CoV

LoVo cells (derived from human colon adenocarcinoma cells) lack furin activity because they harbor two distinct mutant alleles of the furin gene (1286T and 1639C) (19, 20). We purchased LoVo cells from the American Type Culture Collection (ATCC) and quantified expression of mRNA encoding proteins involved in cell entry by MERS-CoV. We confirmed that, like Calu-3 and Huh-7 (derived from human liver carcinoma) cells, LoVo cells expressed DPP4, furin, cathepsin L, and TMPRSS2; however, unlike Calu-3 and Huh-7 cells, LoVo cells expressed HAT (Fig. 3A). Furin expression was highest in Huh-7 cells. We also confirmed deletion and substitution (1286T and 1639C) mutations within the furin mRNA sequence (Fig. 3B) (19, 20). Next, we inoculated MERS-CoV onto LoVo cells and measured virus propagation at 24 h. As reported previously (21), MERS-CoV infected and replicated in LoVo and Calu-3 cells (Fig. 3C). This indicates that furin is not essential for MERS-CoV infection.

Entry of MERS-CoV into furin-deficient LoVo cells

Next, we examined the effect of protease inhibitors on MERS-CoV entry into LoVo cells. E64d suppressed entry of MERS-CoV, but camostat did not, suggesting that the cathepsin/endosomal pathway rather than the TMPRSS2/cell surface pathway is dominant in LoVo cells (Fig. 4A). Treatment with 100 μM dec-RVKR-CMK completely suppressed entry of MERS-CoV, similar to co-treatment with camostat and E64d (Fig. 4A). Furthermore, cell entry by SARS-CoV, in which the S protein lacks furin cleavage sites (13), was also suppressed by dec-RVKR-CMK (Fig. 4B).

MERS-CoV mutants in which the S protein lacks furin cleavage sites at R748 (the S1/S2 site) and/or R884 (the S2' site) were generated using a recently developed reverse genetics system (22). Western blot analysis of S proteins harboring mutations at R748 (R748S or R748S/R884S) detected no 80 kD cleavage product on virions (Fig. 5A, lanes 2 and 4). To characterize the cleavability of these S proteins within cells, Vero/TMPRSS2, Huh-7 (expressing high levels of furin), and LoVo (lacking furin) cells were infected with viruses and cell lysates were examined by western blotting. The S proteins of wt and R884 mutant viruses in Vero/TMPRSS2 and Huh-7 cells were cleaved, but those of R748 mutant viruses (R748S or R748S/R884S) were not (Fig. 5B). By contrast, none of the S proteins were cleaved in LoVo cells (Fig. 5B). This confirmed that LoVo cells lack furin activity and that the R748 mutation in S protein lies within the furin cleavage site. To assess the furin-dependent cell entry of these mutant viruses, they were inoculated onto Huh-7 or LoVo cells and the amount of viral mRNA at 6 h post-infection was measured by real-time PCR. No significant difference was observed between wt and mutant viruses in Huh-7 cells (Fig. 5C), indicating that high levels of furin expressed by these cells did not affect S protein activation during viral entry. Treatment with dec-RVKR-CMK suppressed cell entry by both wt MERS-CoV and mutant MERS-CoV in which the S protein lacks furin cleavage sites (Fig. 5D). These results indicate that entry of furin-deficient cells by virus lacking furin cleavage sites is blocked by the furin inhibitor, suggesting that the molecule targeted by dec-RVKR-CMK during MERS-CoV entry is not furin.

Exogenous furin does not activate the S protein

Next, we examined direct activation of the S protein by exogenous furin. First, we confirmed that commercial furin had the advertised level of activity by testing it using a furin substrate, BOC-RVRR-AMC (Fig. 6A). Treatment with exogenous trypsin, but not

exogenous furin, increased virus entry into LoVo cells (Fig. 6B) and cell-cell fusion by MERS-CoV-infected LoVo cells (Fig. 6C). Therefore, we concluded that furin does not activate the MERS-CoV S protein. In addition, western blot analysis detected very small amounts of cleaved S protein (80 kD) in non-protease-treated viruses propagated in Vero cells (Fig. 6D, lane 1); similar results were obtained for viruses propagated in Vero/TMPRSS2 cells (Fig. 5A). No 80 kD S protein was detected when cells were treated with exogenous furin (2000 units/ml), although the 150 kD and 50 kD products were detected (Fig. 6D, lane 5). Of note, the S protein-harboring virions used for the experiments in Figure 6D were propagated in Vero cells cultured in medium lacking trypsin (a non-enzymatic cell dissociation solution (C5914; Sigma) was used for cell passage). The intensity of the 80 kD band increased only when cells were exposed to exogenous trypsin (0.1 μg/ml) (Fig. 6D, lanes 3 and 7). Therefore, we conclude that the S protein is cleaved by furin during biogenesis, not on virions after exit the cells.

The inhibitor dec-RVKR-CMK targets the early stage of MERS-CoV infection

Our next task was to identify the true target of dec-RVKR-CMK during MERS-CoV infection. First, we examined the effect of dec-RVKR-CMK on endocytosis. pHrodo™ dextran, which is non-fluorescent at neutral pH but exhibits increased fluorescence as the pH becomes acidic, was used as a tracker of endocytic internalization and lysosomal sequestration within live cells. In Calu-3 cells, bafilomycin A1, which blocks acidification of endosomes, clearly inhibited development of pHrodo red, but dec-RVKR-CMK, camostat, and E64d did not (data not shown); this suggests that dec-RVKR-CMK has no effect on endocytosis.

Next, to clarify the time point at which inhibitors block MERS-CoV infection, LoVo cells were treated with 100 μM dec-RVKR-CMK or a mixture of 10 μM E64d and 10 μM camostat (E64d/camostat) during infection with MERS-CoV. Lopinavir, which targets

MERS-CoV 3CL protease and blocks viral RNA replication, was used for comparison. The inhibitors were added at the indicated time points, and cellular RNA was isolated 6 h after infection. Samples collected at 6 h post-infection were used as a control for no inhibitor treatment. The amount of viral mRNA was quantified by real-time PCR. Dec-RVKR-CMK and E64d/camostat showed an inhibitory effect within 30 min after infection (Fig. 7A). By comparison, addition of lopinavir at 2 h post-infection still inhibited the viral RNA replication (Fig. 7A). In Calu-3 cells, dec-RVKR-CMK and E64d/camostat showed a similar effect; both of these inhibitors act at the very early stage of infection (within 30 min) (Fig. 7B). Taken together, the data indicate that dec-RVKR-CMK targets an early step during MERS-CoV entry: potentially S protein activation by TMPRSS2 and cathepsin L.

Inhibitory effect of dec-RVKR-CMK on commercial proteases and TMPRSS2

Next, we examined the inhibitory effect of dec-RVKR-CMK on various proteases. We purchased proteases from commercial sources and tested them using a fluorescent protease assay kit, which measures degradation products of fluorescein-labeled casein. Unfortunately, the kit was unable to detect furin activity because casein does not contain the furin cleavage site. First, 10-fold serially diluted protease was incubated with the substrate to identify the appropriate concentration representing the linear phase of the reaction at 30 min; this was used for the experiments described below. Next, appropriate concentrations of various proteases required to degrade the substrate were mixed with dec-RVKR-CMK and inhibition kinetics were measured. Figure 8A shows that a high concentration (100 μM) of dec-RVKR-CMK completely suppressed the activity of cathepsin L, cathepsin B, trypsin, and papain, partially suppressed that of proteinase K and dispase, and slightly suppressed that of elastase and chymotrypsin. Neither E64d nor bafilomycin A1 (used as a control) suppressed the activity of trypsin, chymotrypsin, or

elastase (Fig. 8B).

To examine the inhibitory effect of dec-RVKR-CMK on TMPRSS2, we performed a fusion-from-without (FFWO) assay as described previously (10). This assay detects viral S protein-mediated cell-cell fusion activated by TMPRSS2 on the cell surface; the assay excludes the effects of inhibitors on virus replication, meaning that it detects TMPRSS2 activity directly. Briefly, a high titer (MOI = 10) of MERS-CoV was adsorbed onto Vero/TMPRSS2 cells on ice for 1 h. The cells were then shifted to 37°C in the presence or absence of inhibitors. Cell-cell fusion was first observed at 3 h after warming. The dec-RVKR-CMK inhibitor (100 μM) suppressed cell-cell fusion completely, as did camostat (10 μM; used as the control) (Fig. 8C). These results strongly suggest that dec-RVKR-CMK targets cell surface TMPRSS2, which plays a role in cell entry by MERS-CoV.

DISCUSSION

Cellular furin plays a role in virus infection and numerous other biological phenomena, most of which were identified by experimental observations using the furin inhibitor dec-RVKR-CMK (11, 13, 23–25). However, the results presented herein indicate that dec-RVKR-CMK inhibited not only furin but also cathepsin L and TMPRSS2 (Fig. 8A and C). In addition, we observed that dec-RVKR-CMK blocked entry of viruses harboring an S protein lacking furin cleavage sites; it even blocked entry into furin-deficient LoVo cells (Fig. 5D). This suggests that the results of previous studies using dec-RVKR-CMK may have to be re-examined.

In addition, virus entry or cell-cell fusion assays provided no evidence that the S protein was activated by exogenous furin (Fig. 6B and C). A previous study claims to show direct evidence of S protein activation by furin because induction of cell-cell fusion in S protein-expressing Huh-7 cells was observed after removing dec-RVKR-CMK from the

250 culture medium and adding exogenous furin (13). However, exogenous furin may not be
251 required to induce cell-cell fusion of Huh-7 cells because these cells induce cell-cell
252 fusion after MERS-CoV infection in the absence of proteases (26).
253 Here, we discuss the use of host proteases by MERS-CoV for cell entry. Studies show
254 clearly that TMPRSS2 activates the MERS-CoV S protein (4, 10, 27). Expression of
255 TMPRSS2 at the cell surface induces both virus entry into cells and cell-cell fusion of S
256 protein-expressing cells (4, 10, 27). Furthermore, these phenomena are suppressed by the
257 serine protease inhibitors camostat mesylate and nafamostat mesylate (4, 10, 28). In
258 addition, other extracellular proteases such as trypsin and elastase activate the
259 MERS-CoV S protein in a manner similar to TMPRSS2 (10).
260 However, cathepsin L usage by MERS-CoV remains controversial because there is no
261 clear evidence that the S protein is activated by exposure to exogenous cathepsin L. A
262 previous study shows that cell-cell fusion induced by exogenous cathepsin L in
263 SARS-CoV S protein-expressing cells is insufficient (29). Also, our previous study shows
264 that cathepsin L requires chlorpromazine, a membrane-permeable cationic drug that
265 lowers the energy requirement for membrane fusion, to induce a small increase in cell
266 entry by murine coronavirus (30). Therefore it is unclear whether cathepsin L plays a role
267 in activating the coronavirus S protein. However, it is at least certain that the enzymatic
268 activity of cathepsin is necessary for proteolytic activation of the MERS-CoV cell entry
269 because expression of TMPRSS2 overcomes blockade of viral cell entry by cathepsin
270 inhibitors (10).
271 Taken together, the results presented herein do not support a role for cellular furin during
272 direct activation of MERS-CoV S protein for viral cell entry. These findings are
273 compatible with those of a previous study by Gierer et al. showing that MERS-CoV does
274 not require furin for infectivity (14). Park et al. report that the only role played by furin
275 during MERS-CoV infection is to determine the cell tropism of the virus (8). What is

certain that the MERS-CoV S protein pre-cleaved by furin at the S1/S2 site still requires cell surface/extracellular and endosomal proteases such as TMPRSS2, elastase, and cathepsin L, for cleavage at the S2' site.

MATERIALS AND METHODS

Cells and viruses

LoVo and Calu-3 cell lines were cultured as recommended by the ATCC. Vero cells obtained from the ATCC and Vero cells expressing TMPRSS2 (Vero/TMPRSS2) (18) were maintained in Dulbecco's Modified Eagle Medium (DMEM; Sigma-Aldrich, USA) supplemented with 5% heat-inactivated fetal bovine serum (Gibco-BRL, USA). MERS-CoV EMC strain and SARS-CoV Frankfurt 1 strain were propagated in Vero cells.

Generation of a pseudotyped virus

The VSV-pseudotyped virus expressing GFP or luciferase and harboring the MERS-CoV S protein was prepared as previously described (31). Briefly, at 24 h post-transfection with pKS-MERS-St16, 293T cells were infected with VSVΔG-G/GFP or VSVΔG-G/Luc at a MOI of 0.1. After absorption for 1 h, the inoculum was replaced with culture medium. After a further incubation for 24 h, the culture supernatants were collected and stored at -80°C. The titer of VSV-pseudotyped viruses was determined in Vero cells. For the VSV-pseudotyped virus expressing GFP, images were captured under a BZ8000 microscope (Keyence, Japan) and GFP-positive cells were counted using image measurement and analysis software (VH-H1A5 version 2.6; Keyence). For the VSV-pseudotyped virus expressing luciferase, cells were lysed and assayed for luciferase activity using a luciferase assay kit (Promega, USA) and a Glomax 20/20 luminometer

instrument (Promega).

Generation of recombinant MERS-CoV from bacterial artificial chromosome (BAC) plasmids

A bacterial artificial chromosome (BAC) clone carrying the full-length infectious genome of the MERS-CoV EMC2012 strain (termed pBAC-MERS-wt) was used to generate recombinant MERS-CoV (22). Amino acid substitutions at the P1 site within the fusion cleavage sites in the S protein were generated by modification of the pBAC-MERS-wt (the template) using a Red/ET Recombination System Counter-Selection BAC Modification Kit (Gene Bridges, Heidelberg, Germany). This yielded pBAC-MERS-S/R748S, pBAC-MERS-S/R884S, and pBAC-MERS-S/R748S/R884S. Huh-7 cells were grown to approximately 60% confluence in a 6-well plate (VIOLAMO, Japan) and then transfected with 4 µg of the indicated BAC DNA using the X-tremeGENE 9 DNA Transfection Reagent (Roche). Transfected cells were cultured at 37°C for the indicated times, and the culture supernatants and cell pellets were collected. The culture supernatants were inoculated onto a 10 cm dish (VIOLAMO) containing Huh-7 cells and cultured overnight. Infected cells were incubated at 37°C for 3 or 4 days until a cytopathic effect (CPE) was observed. Culture supernatants were collected, centrifuged at 2500×g for 5 min at 4°C, and stored at -80°C.

Proteases and protease inhibitors

The following proteases were used: cathepsin L (16-12-030112; Athens, USA), cathepsin B (16-12-030102; Athens), trypsin (T8802; Sigma, USA), papain (53J6521; Worthington, USA), proteinase K (166-21051; Wako, Japan), dispase (1 276 921; Roche, Switzerland), elastase (Sigma; E-0258), chymotrypsin (Sigma; C-3142), and furin (P8077; NEB, UK). The following inhibitors were used: dec-RVKR-CMK (3501; Tocris, UK), E64d (330005;

Calbiochem, USA), camostat (3193; Tocris Bioscience, UK), bafilomycin A1 (B1793; Sigma), and lopinavir (SML1222; Sigma).

Cell entry assay for authentic MERS-CoV

Confluent cells in 96-well plates were pretreated for 30 min with inhibitors. Cells were then inoculated with MERS-CoV and incubated (with the inhibitors) for 1 h on ice, followed by culture at 37°C for 6 h. Cellular RNA was isolated by addition of Isogen reagent (315-02504; Nippon Gene, Japan). A real-time PCR assay was performed to quantify the amount of newly synthesized subgenomic MERS-CoV RNA using the primers and probes described previously (10). PCR analysis was performed in a LightCycler-Nano instrument (Roche Diagnostics, Switzerland).

Quantification of transcripts in LoVo cells

Total RNA was isolated from LoVo cells using the Isogen reagent. Real-time PCR was performed to quantify expression of mRNA encoding GAPDH, DPP4, furin, cathepsin L, TMPRSS2, and HAT using the primers and probes described previously (10). Comparative expression of mRNA was calculated from a calibration line obtained by stepwise dilution (10-fold) of RNA samples.

Quantification of furin activity

Recombinant human furin (P8077; New England Biolabs, UK) was mixed with 100 μM furin substrate (boc-RVRR-AMC; I-1645; Bachem, Switzerland) in phosphate buffered saline containing 1 mM $CaCl_2$ (32). After 30 min at 37°C, fluorescence analysis was performed using a Power Scan HT instrument (DS Pharma, Japan) fitted with fluorescein excitation/emission filters (360/480 nm).

354

355 **Western blot analysis**

356 To detect cleaved S protein in virions, viral supernatant was mixed with recombinant
357 human furin (P8077; New England Biolabs) or trypsin (T-8802; Sigma) in furin reaction
358 buffer (20 mM HEPES, pH 7.5, 0.1% Triton X-100, 0.2 mM $CaCl_2$, and 0.2 mM
359 β-mercaptoethanol) and incubated at 37°C for 1 h. One quarter volume of sample buffer
360 (30% glycerol, 250 mM Tris pH 6.8, 2.5% SDS, a small amount of Bromophenol blue,
361 100 mM DTT, and 1 mM pefablock SC) was added to the reaction and boiled for 5 min.
362 Samples were loaded onto SDS-PAGE (3–10% gradient) gels (e-PAGEL; ATTO, Japan),
363 transferred to a PVDF membrane (Immobilon-P; Millipore, USA), and soaked in
364 ImmunoBlock (CTKN001; DS Pharma Biomedical, Japan). Western blot analysis was
365 carried out using an anti-S2 antibody and anti-rabbit IgG (sc-2054; Santa Cruz Biotech,
366 USA). Immunoreactive bands were visualized with an enhanced chemiluminescence kit
367 (ECL, RPN2232; GE Healthcare, USA) and a LAS-3000 instrument (Fuji, Japan).
368 To detect the S protein in MERS-CoV-infected cells, cells were dissolved in sample
369 buffer and subjected to western blot analysis as described above. After detection by an
370 anti-S2 antibody, the membrane was soaked in stripping buffer (46428; ThermoFisher,
371 USA) for 5 min at room temperature to remove the antibodies and then rinsed 10 times
372 with rinse buffer (20845; Millipore). The membrane was then blocked and re-probed with
373 an anti-GAPDH antibody (IMG-5143A; IMGENEX, USA), followed by anti-rabbit IgG.

374

375 **Fluorescent protease assay for commercial proteases**

376 The activity of the proteases listed above was quantified using a fluorescent protease
377 assay kit (23266; Pierce, USA), which measures the degradation products of
378 fluorescein-labeled casein. To measure the activity of neutral pH-dependent proteases
379 (trypsin, papain, proteinase K, dispase, elastase, and chymotrypsin), experiments were

carried out according to the manufacturer's protocol. To measure the activity of low pH-dependent cathepsin L and cathepsin B, the substrate (which has neutral pH-dependent fluorescence) was first dissolved in low pH buffer (50 mM sodium acetate pH 5.0, 1 mM EDTA, and 5 mM DTT). After a 30 min incubation with cathepsin at 37°C, 1/20 volume of 1 M Tris-HCl buffer pH 8.0 was added to render the fluorescein detectable at neutral pH. Fluorescence analysis was performed using a Power Scan HT instrument (DS Pharma, Japan) fitted with fluorescein excitation/emission filters (485/528 nm).

FFWO assay

The FFWO assay was performed as previously described (10). Briefly, Vero/TMPRSS2 cells (10^5 cells) in 96-well plates were inoculated with a high titer (10^6 PFU) of authentic MERS-CoV. Cells were then incubated at 37°C in the presence of inhibitors. After incubation for 5 h, cells were fixed with 4% formaldehyde and stained with crystal violet.

Statistical analysis

Statistical significance was assessed using a two-tailed Student t test. A p-value <0.05 was considered statistically significant. n.s. = not significant, * = significant ($p \leq 0.05$), ** = highly significant ($p \leq 0.01$), *** = very highly significant ($p \leq 0.001$). Error bars indicate the SD.

ACKNOWLEDGMENT

We thank Ron A. M. Fouchier (Erasmus Medical Center, Rotterdam, The Netherlands) for providing the MERS-CoV EMC strain, and John Ziebuhr (University of Würzburg, Würzburg, Germany) for providing the SARS-CoV Frankfurt 1 strain. We also thank Aiko Fukuma and Hideki Tani (NIID, Japan) for valuable suggestions. This study was

supported by a Grant-in-Aid for Scientific Research from the Japan Society for the Promotion of Science (Grant No. 17K08868).

REFERENCES

1. **White JM**, **Whittaker GR**. 2016. Fusion of Enveloped Viruses in Endosomes. Traffic **17**:593–614.
2. **Heald-Sargent T**, **Gallagher T**. 2012. Ready, set, fuse! the coronavirus spike protein and acquisition of fusion competence. Viruses **4**:557–580.
3. **Millet JK**, **Whittaker GR**. 2015. Host cell proteases: Critical determinants of coronavirus tropism and pathogenesis. Virus Res. **202**:120–134.
4. **Gierer S**, **Bertram S**, **Kaup F**, **Wrensch F**, **Heurich A**, **Krämer-Kühl A**, **Welsch K**, **Winkler M**, **Meyer B**, **Drosten C**, **Dittmer U**, **von Hahn T**, **Simmons G**, **Hofmann H**, **Pöhlmann S**. 2013. The spike protein of the emerging betacoronavirus EMC uses a novel coronavirus receptor for entry, can be activated by TMPRSS2, and is targeted by neutralizing antibodies. J. Virol. **87**:5502–11.
5. **Simmons G**, **Reeves JD**, **Rennekamp AJ**, **Amberg SM**, **Piefer AJ**, **Bates P**. 2004. Characterization of severe acute respiratory syndrome-associated coronavirus (SARS-CoV) spike glycoprotein-mediated viral entry. Proc. Natl. Acad. Sci. U. S. A. **101**:4240–4245.
6. **Belouzard S**, **Chu VC**, **Whittaker GR**. 2009. Activation of the SARS coronavirus spike protein via sequential proteolytic cleavage at two distinct sites. Proc. Natl. Acad. Sci. U. S. A. **106**:5871–5876.
7. **Watanabe R**, **Matsuyama S**, **Shirato K**, **Maejima M**, **Fukushi S**, **Morikawa S**, **Taguchi F**. 2008. Entry from the cell surface of severe acute respiratory syndrome coronavirus with cleaved S protein as revealed by pseudotype virus bearing cleaved S protein. J. Virol. **82**:11985–11991.
8. **Park J-E**, **Li K**, **Barlan A**, **Fehr AR**, **Perlman S**, **McCray PB**, **Gallagher T**. 2016. Proteolytic processing of Middle East respiratory syndrome coronavirus spikes expands virus tropism. Proc. Natl. Acad. Sci. **113**:12262–12267.
9. **Reinke LM**, **Spiegel M**, **Plegge T**, **Hartleib A**, **Nehlmeier I**, **Gierer S**, **Hoffmann M**, **Hofmann-winkler H**, **Winkler M**, **Pöhlmann S**. 2017. Different residues in the SARS-CoV spike protein determine cleavage and activation by the host cell protease TMPRSS2. PLoS One **12(6)**:e0179177.
10. **Shirato K**, **Kawase M**, **Matsuyama S**. 2013. Middle East respiratory syndrome

coronavirus infection mediated by the transmembrane serine protease TMPRSS2. J. Virol. **87**:12552–61.

11. **Thomas G**. 2002. Furin at the cutting edge: from protein traffic to embryogenesis and disease. Nat. Rev. Mol. Cell Biol. **3**:753–66.
12. **Burkard C**, **Verheije MH**, **Wicht O**, **van Kasteren SI**, **van Kuppeveld FJ**, **Haagmans BL**, **Pelkmans L**, **Rottier PJM**, **Bosch BJ**, **de Haan C a. M**. 2014. Coronavirus Cell Entry Occurs through the Endo-/Lysosomal Pathway in a Proteolysis-Dependent Manner. PLoS Pathog. **10**:e1004502.
13. **Millet JK**, **Whittaker GR**. 2014. Host cell entry of Middle East respiratory syndrome coronavirus after two-step, furin-mediated activation of the spike protein. Proc. Natl. Acad. Sci. U. S. A. **111**:15214–9.
14. **Gierer S**, **Muller MA**, **Heurich A**, **Ritz D**, **Springstein BL**, **Karsten CB**, **Schendzielorz A**, **Gnirss K**, **Drosten C**, **Pohlmann S**. 2015. Inhibition of Proprotein Convertases Abrogates Processing of the Middle Eastern Respiratory Syndrome Coronavirus Spike Protein in Infected Cells but Does Not Reduce Viral Infectivity. J. Infect. Dis. **211**:889–897.
15. **Coppola JM**, **Bhojani MS**, **Ross BD**, **Rehemtulla A**. 2008. A Small-Molecule Furin Inhibitor Inhibits Cancer Cell Motility and Invasiveness. Neoplasia **10**:363–370.
16. **Becker GL**, **Lu Y**, **Hardes K**, **Strehlow B**, **Levesque C**, **Lindberg I**, **Sandvig K**, **Bakowsky U**, **Day R**, **Garten W**, **Steinmetzer T**. 2012. Highly potent inhibitors of proprotein convertase furin as potential drugs for treatment of infectious diseases. J. Biol. Chem. **287**:21992–2003.
17. **Basak A**. 2005. Inhibitors of proprotein convertases. J. Mol. Med. **83**:844–855.
18. **Shirogane Y**, **Takeda M**, **Iwasaki M**, **Ishiguro N**, **Takeuchi H**, **Nakatsu Y**, **Tahara M**, **Kikuta H**, **Yanagi Y**. 2008. Efficient multiplication of human metapneumovirus in Vero cells expressing the transmembrane serine protease TMPRSS2. J. Virol. **82**:8942–8946.
19. **Takahashi S**, **Kasai K**, **Hatsuzawa K**, **Kitamura N**, **Misumi Y**, **Ikehara Y**, **Murakami K**, **Nakayama K**. 1993. A Mutation of Furin Causes the Lack of Precursor-Processing Activity in Human Colon Carcinoma LoVo Cells. Biochem. Biophys. Res. Commun. **195**:1019–1026.
20. **Takahashi S**, **Nakagawa T**, **Kasai K**, **Banno T**, **Duguay SJ**, **Ven WJM Van De**, **Murakami K**, **Nakayama K**. 1995. A Second Mutant Allele of Furin in the Processing-incompetent Cell Line , LoVo. J. Biol. Chem. **270**:26565–26569.

21. **Tao X**, **Hill TE**, **Morimoto C**, **Peters CJ**, **Ksiazek TG**, **Tseng C-TK**. 2013. Bilateral entry and release of Middle East respiratory syndrome coronavirus induces profound apoptosis of human bronchial epithelial cells. J. Virol. **87**:9953–8.
22. **Terada Y**, **Kawachi K**, **Matsuura Y**, **Kamitani W**. 2017. MERS coronavirus nsp1 participates in an efficient propagation through a specific interaction with viral RNA. Virology **511**:95–105.
23. **Haan CAM De**, **Stadler K**, **Godeke G**, **Bosch BJ**, **Rottier PJM**. 2004. Cleavage Inhibition of the Murine Coronavirus Spike Protein by a Furin-Like Enzyme Affects Cell-Cell but Not Virus-Cell Fusion. J. Virol. **78**:6048–6054.
24. **Couture F**, **D'Anjou F**, **Day R**. 2011. On the cutting edge of proprotein convertase pharmacology: from molecular concepts to clinical applications. Biomol. Concepts **2**:421–438.
25. **Klein-Szanto AJ**, **Bassi DE**. 2017. Proprotein convertase inhibition: Paralyzing the cell's master switches. Biochem. Pharmacol. **140**:8–15.
26. **de Wilde AH**, **Raj VS**, **Oudshoorn D**, **Bestebroer TM**, **van Nieuwkoop S**, **Limpens RW a L**, **Posthuma CC**, **van der Meer Y**, **Bárcena M**, **Haagmans BL**, **Snijder EJ**, **van den Hoogen BG**. 2013. MERS-coronavirus replication induces severe in vitro cytopathology and is strongly inhibited by cyclosporin A or interferon-α treatment. J. Gen. Virol. **94**:1749–1760.
27. **Barlan A**, **Zhao J**, **Sarkar MK**, **Li K**, **McCray PB**, **Perlman S**, **Gallagher T**. 2014. Receptor variation and susceptibility to Middle East respiratory syndrome coronavirus infection. J. Virol. **88**:4953–61.
28. **Yamamoto M**, **Matsuyama S**, **Li X**, **Takeda M**, **Kawaguchi Y**, **Inoue J**, **Matsuda Z**. 2016. Identification of Nafamostat as a Potent Inhibitor of Middle East Respiratory Syndrome Coronavirus S Protein-Mediated Membrane Fusion Using the Split-Protein-Based Cell-Cell Fusion Assay. Antimicrob. Agents Chemother. **60**:6532–6539.
29. **Bosch BJ**, **Bartelink W**, **Rottier PJM**. 2008. Cathepsin L functionally cleaves the severe acute respiratory syndrome coronavirus class I fusion protein upstream of rather than adjacent to the fusion peptide. J. Virol. **82**:8887–8890.
30. **Matsuyama S**, **Taguchi F**. 2009. Two-step conformational changes in a coronavirus envelope glycoprotein mediated by receptor binding and proteolysis. J. Virol. **83**:11133–11141.
31. **Fukuma A**, **Tani H**, **Taniguchi S**, **Shimojima M**, **Saijo M**, **Fukushi S**. 2015.

Inability of rat DPP4 to allow MERS-CoV infection revealed by using a VSV pseudotype bearing truncated MERS-CoV spike protein. Arch. Virol. **160**:2293–300.

32. **Komiyama T**, **Coppola JM**, **Larsen MJ**, **van Dort ME**, **Ross BD**, **Day R**, **Rehemtulla A**, **Fuller RS**. 2009. Inhibition of furin/proprotein convertase-catalyzed surface and intracellular processing by small molecules. J. Biol. Chem. **284**:15729–15738.

538

539

540

541 **FIGURE LEGENDS**

542 **Fig. 1. Comparison of three assays to quantify virus cell entry.**

543 (A–C) Cell entry by pseudotyped or authentic MERS-CoV. Vero/TMPRSS2 cells in
544 96-well plates were infected with the serially diluted viruses indicated below. The
545 relationship between inoculated virus titer (x-axis) and data values (average of two
546 experiments) for each assay (y-axis) is shown.

547 (A) VSV-ΔG/GFP-MERS-S. GFP-positive cells were counted at 20 h post-infection.

548 (B) VSV-ΔG/Luc-MERS-S. Luciferase activity in cells was measured at 20 h
549 post-infection.

550 (C) Authentic MERS-CoV. The amount of viral mRNA in cells at 6 h post-infection was
551 measured by real-time PCR.

552 (D–F) Effect of a furin inhibitor on cell entry by pseudotyped or authentic MERS-CoV.
553 Vero/TMPRSS2 cells were inoculated with viruses in the presence or absence of the furin
554 inhibitor dec-RVKR-CMK. Virus entry was measured using appropriate assays.

555 (D) Effect of dec-RVKR-CMK on cell entry by VSV-ΔG/GFP-MERS-S. Cells were
556 inoculated with 10^3 infectious units of VSV-ΔG/GFP-MERS-S (MOI = 0.01).
557 GFP-positive cells were counted at 20 h post-infection (n = 4).

558 (E) Effect of dec-RVKR-CMK on cell entry by VSV-ΔG/Luc-MERS-S. Cells were
559 inoculated with 10^4 infectious units of VSV-ΔG/Luc-MERS-S (MOI = 0.1). Luciferase
560 activity in cells was measured at 20 h post-infection (n = 4). Data are presented on a
561 linear (left panel) and a logarithmic (right panel) scale.

562 (F) Effect of dec-RVKR-CMK on cell entry by authentic MERS-CoV. Cells were
563 inoculated with 10^5 infectious units of authentic MERS-CoV (MOI = 1). The amount of

viral mRNA in cells at 6 h post-infection was measured by real-time PCR (n = 4). A two-tailed Student t test was used to analyze statistical significance. n.s. = not significant, * = significant ($p \leq 0.05$), ** = highly significant ($p \leq 0.01$), *** = very highly significant ($p \leq 0.001$). Error bars indicate the standard deviation (SD). ND = not detected.

Fig. 2. Effect of a furin inhibitor on MERS-CoV entry into Calu-3 cells.

Calu-3 human bronchial epithelial cells were pretreated for 30 min with increasing concentrations (0–100 μM) of the furin inhibitor dec-RVKR-CMK. E64d (10 μM), camostat (10 μM), or a combination of both was used as a comparison control. The cells were then infected with 10^5 plaque-forming units (pfu) of MERS-CoV (MOI = 1) in the presence of inhibitor. The amount of viral mRNA in Calu-3 cells at 6 h post-infection was measured by real-time PCR (n = 4). A two-tailed Student t test was used to analyze statistical significance, as described in the legend to Figure 1. Error bars indicate the SD.

Fig. 3. Comparison of transcripts in LoVo cells.

(A) Expression of mRNA in Calu-3, LoVo, and Huh-7 cells. Total cellular RNA (0.1 μg) was evaluated for expression of GAPDH, DPP4, furin, cathepsin L, TMPRSS2, and HAT transcripts using real-time PCR (n = 4). ND, no transcripts were detected.

(B) Electropherograms of furin cDNA. The mRNAs isolated from Calu-3 and LoVo cells were reverse-transcribed and amplified using a thermal cycler and used for DNA sequencing.

(C) Viral yield in LoVo cells. Confluent Calu-3 cells and LoVo cells were grown in 96-well plates and infected with MERS-CoV at a MOI of 0.001 for 24 h. Cell-free supernatants were harvested, and infectious viral titers were measured in a standard plaque assay using Vero/TMPRSS2 cells (n = 4).

A two-tailed Student t test was used to analyze statistical significance, as described in the legend to Figure 1. Error bars indicate the SD.

Fig. 4. Effect of furin inhibitor on MERS-CoV and SARS-CoV entry into LoVo cells.

(A) Effect of inhibitors on MERS-CoV entry. LoVo cells were pretreated for 30 min with the furin inhibitor dec-RVKR-CMK (concentration, 0–100 μM). E64d (10 μM), camostat (10 μM), or a combination of both was used as a comparison control. The cells were then infected with 10^5 pfu of MERS-CoV (MOI = 1) in the presence of inhibitor. The amount of viral mRNA in LoVo cells at 6 h post-infection was measured by real-time PCR (n = 4).

(B) Effect of inhibitors on SARS-CoV entry. SARS-CoV was used instead of MERS-CoV; all experiments were carried out as described in panel A.

A two-tailed Student t test was used to analyze statistical significance, as described in the legend to Figure 1. Error bars indicate the SD.

Fig. 5. Effect of mutations in the furin cleavage site of the MERS-CoV S protein.

(A) Cleavage of the S protein on virions. Wild-type (wt) and mutant MERS-CoV lacking furin cleavage sites within the S protein (generated in Vero/TMPRSS2 cells) were subjected to western blot analysis with an anti-S polyclonal antibody.

(B) Cleavage of S protein in cells. The wt and mutant viruses shown in panel A were used to infect Vero/TMPRSS2, Huh-7, and LoVo cells, and cell lysates prepared at 20 h post-infection were subjected to western blot analysis.

(C) Entry of mutant viruses into LoVo and Huh-7 cells. The cells were infected with 10^4 pfu of MERS-CoV (MOI = 0.1). The amount of viral mRNA in cells at 6 h post-infection was measured by real-time PCR (n = 4).

(D) Effect of mutations on virus entry. LoVo cells were pretreated for 30 min with the

616 furin inhibitor dec-RVKR-CMK (concentration at 100 μM). Then, cells were infected
617 with 10^4 pfu of MERS-CoV (MOI = 0.1) in the presence of inhibitor. The amount of viral
618 mRNA in cells at 6 h post-infection was measured by real-time PCR (*n* = 4). Data are
619 expressed as the -fold change in viral mRNA levels relative to that in the absence of
620 dec-RVKR-CMK.
621 A two-tailed Student t test was used to analyze statistical significance, as described in the
622 legend to Figure 1. Error bars indicate the SD.
623
624 **Fig. 6. S protein activation by exogenous furin.**
625 (A) Activity of commercial furin. The enzymatic activity of recombinant human furin
626 used in the experiment below was confirmed using the fluorescent substrate
627 BOC-RVRR-AMC.
628 (B) Exogenous furin does not trigger cell entry by virus. LoVo cells in 96-well plates
629 were inoculated with MERS-CoV (MOI of 0.1) for 30 min and then treated with furin
630 (2000 units/ml) or trypsin (10 μg/ml) at 37°C for 10 min. Cells were then cultured at
631 37°C for 6 h. The amount of viral mRNA was measured by real-time PCR (*n* = 4). A
632 two-tailed Student t test was used to analyze statistical significance, as described in the
633 legend to Figure 1. Error bars indicate the SD.
634 (C) Exogenous furin does not induce syncytium formation. LoVo cells infected with
635 MERS-CoV (MOI of 0.01) were cultured for 20 h and then treated with furin (2000
636 units/ml) or trypsin (10 μg/ml) for 5 h.
637 (D) Cleavage of S protein by exogenous furin. MERS-CoV propagated in Vero cells was
638 treated with the indicated concentrations of trypsin or furin at 37°C for 60 min. Western
639 blot analysis was performed using an anti-S polyclonal antibody.
640
641 **Fig. 7. Timing of inhibitor addition to block entry of MERS-CoV into cells.**

(A) Dec-RVKR-CMK (100 μM), camostat (10 μM) plus E64d (10 μM), or lopinavir (30 μM) was added to LoVo cells (for 30 min on ice) at the indicated times before and after MERS-CoV inoculation. The amount of viral mRNA in cells at 6 h post-infection was measured by real-time PCR (*n* = 1).

(B) Calu-3 cells were used instead of LoVo cells; all experiments were carried out as described in panel A (excluding lopinavir treatment) (*n* = 1).

Fig. 8. Effect of furin inhibitor on commercial proteases and cell surface TMPRSS2.

(A) Inhibitory effect of dec-RVKR-CMK on commercial proteases. Degradation products of fluorescein-labeled casein generated by treatment with commercial proteases, cathepsin L (20 μg/ml), cathepsin B (20 μg/ml), trypsin (50 μg/ml), papain (0.3 units/ml), proteinase K (0.3 units/ml), dispase (3 units/ml), elastase (200 μg/ml), and chymotrypsin (10 μg/ml), at 37°C for 30 min in the presence of dec-RVKR-CMK (serially diluted 10-fold) were quantified by fluorometry (*n* = 3). Data are expressed as an average percentage relative to that in the absence of dec-RVKR-CMK. N, no inhibitor treatment.

(B) E64d and bafilomycin A1 do not inhibit commercial proteases. E64d or bafilomycin A1 was used instead of dec-RVKR-CMK; all experiments were carried out as described in panel A (proteases tested were trypsin, chymotrypsin, and elastase).

(C) Inhibitory effect of dec-RVKR-CMK against TMPRSS2, as assessed in the FFWO assay. A high titer of MERS-CoV (MOI = 10) was adsorbed onto Vero/TMPRSS2 or Vero cells (on ice for 1 h). Cells were then incubated at 37°C in the presence of the inhibitor. After 5 h, cells were fixed and stained with crystal violet.

Figure 1

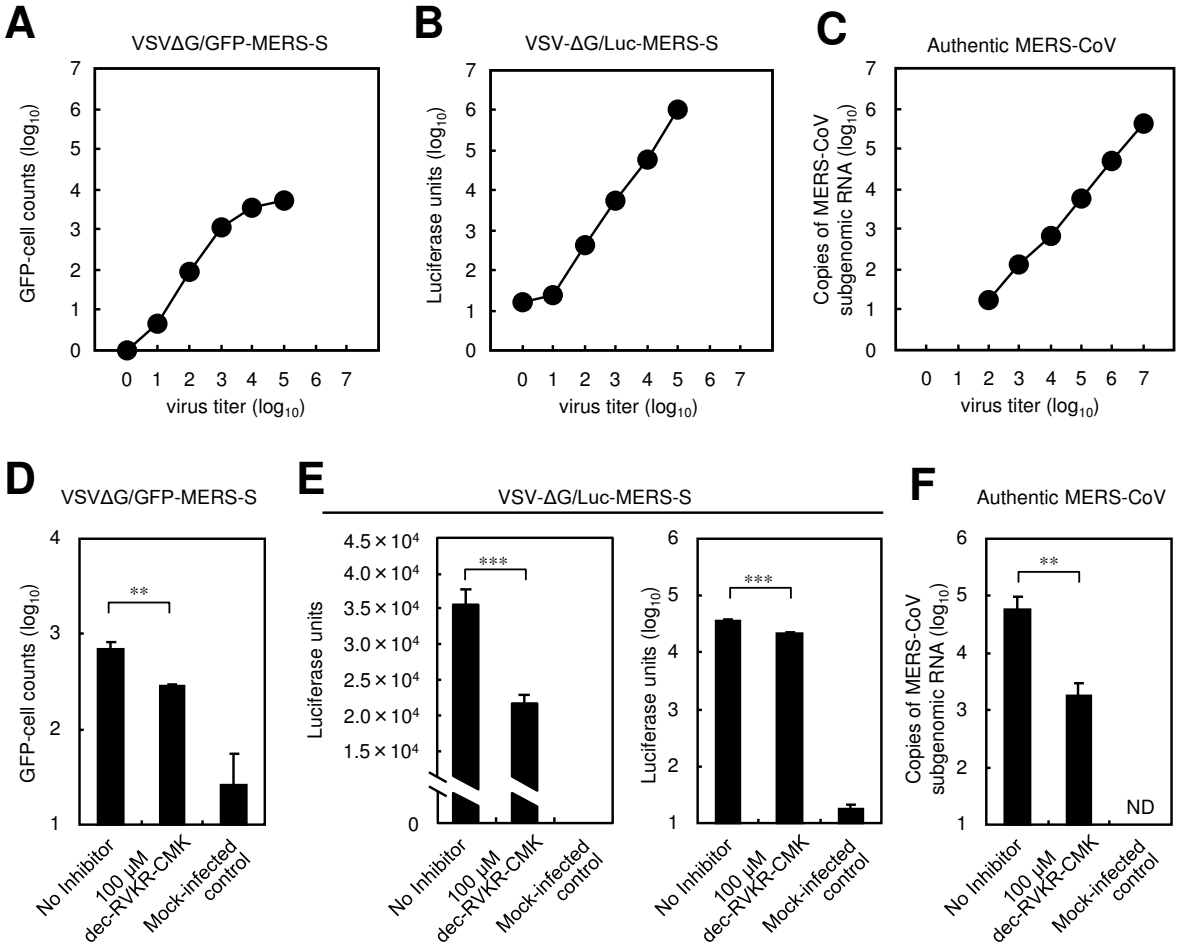

Figure 2

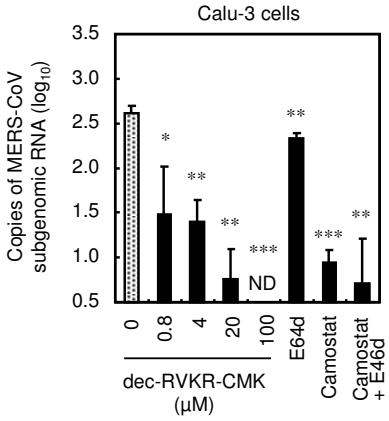

Figure 3

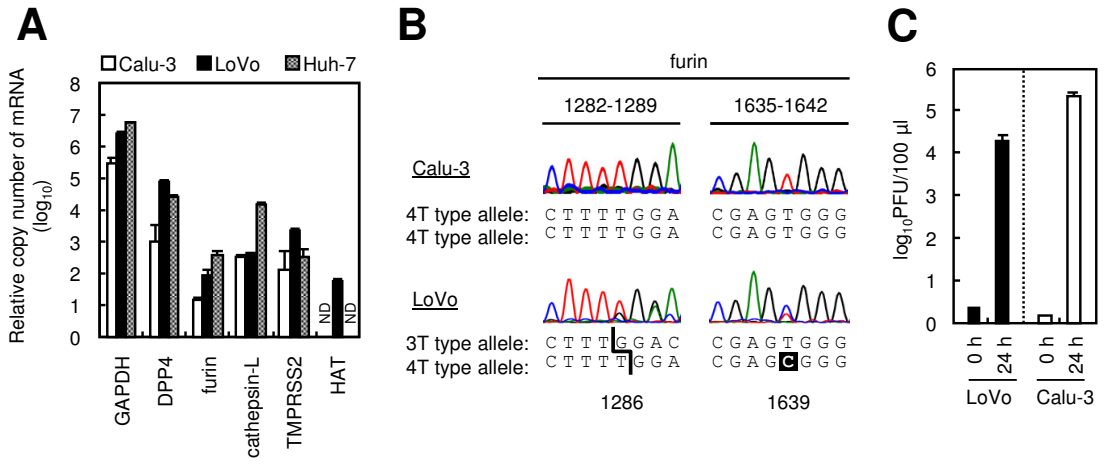

Figure 4

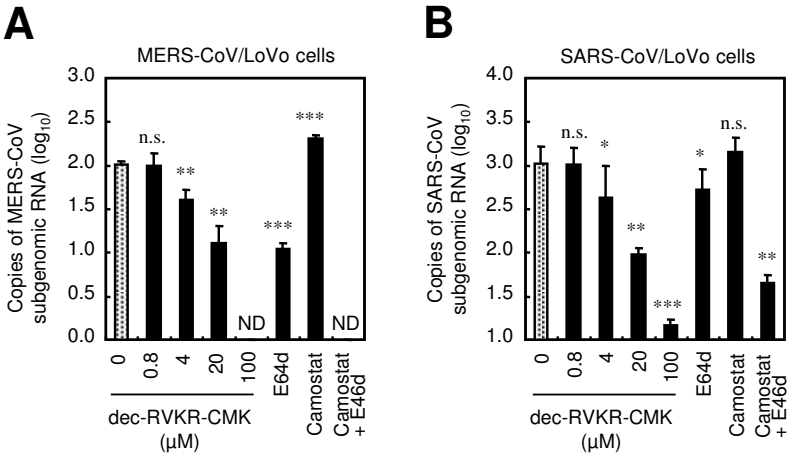

Figure 5

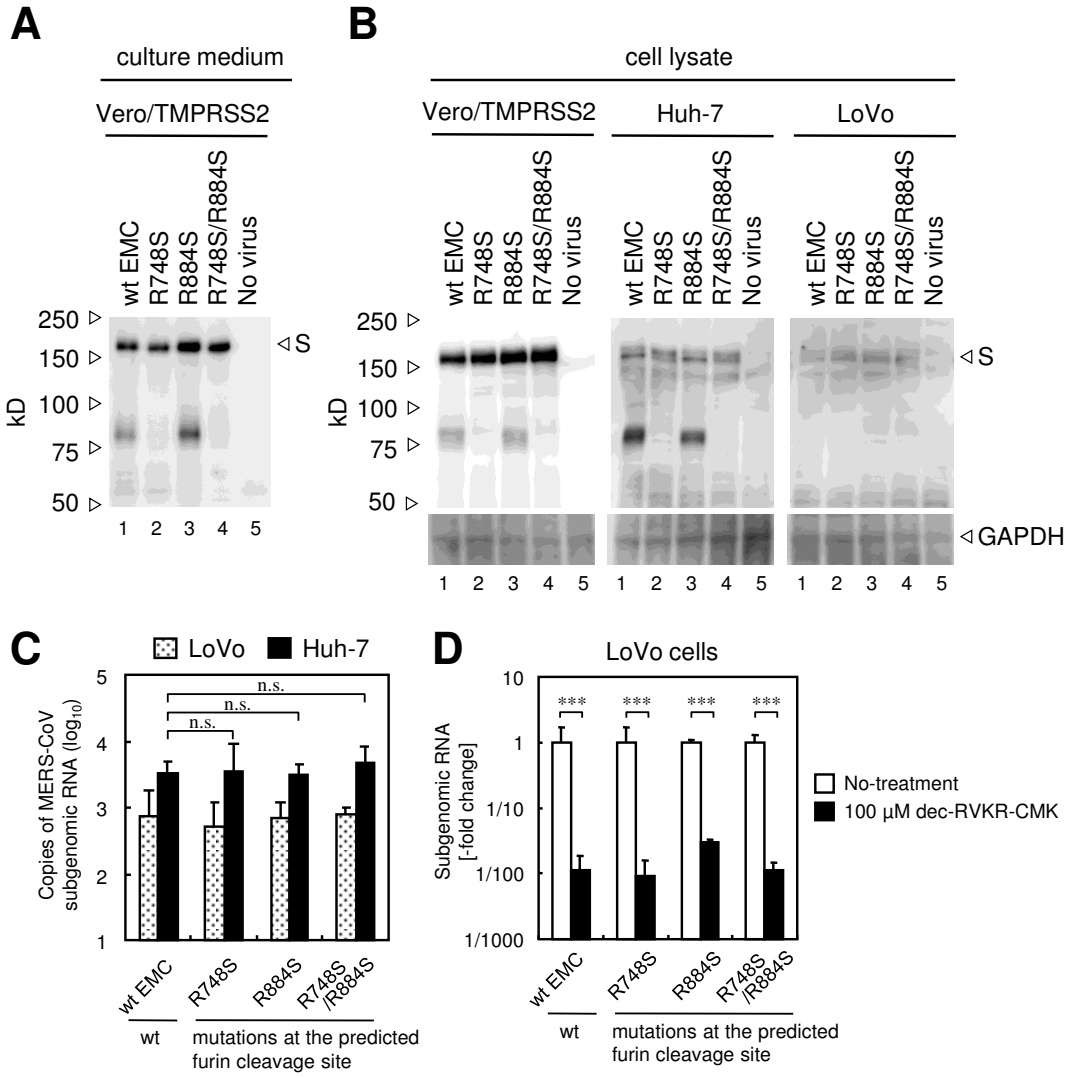

Figure 6

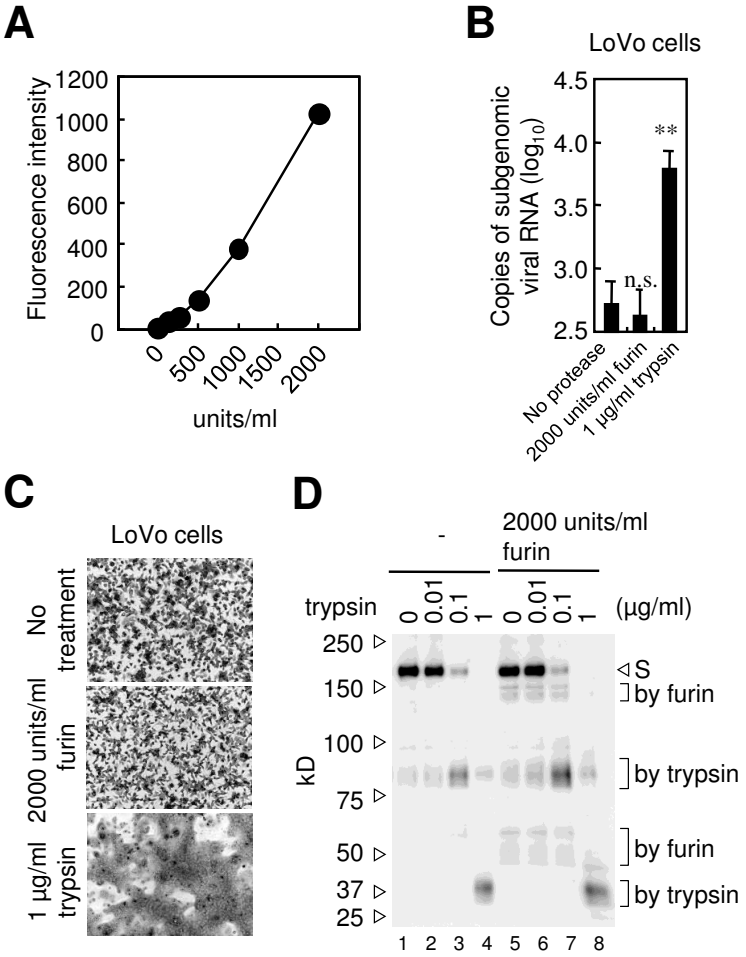

Figure 7

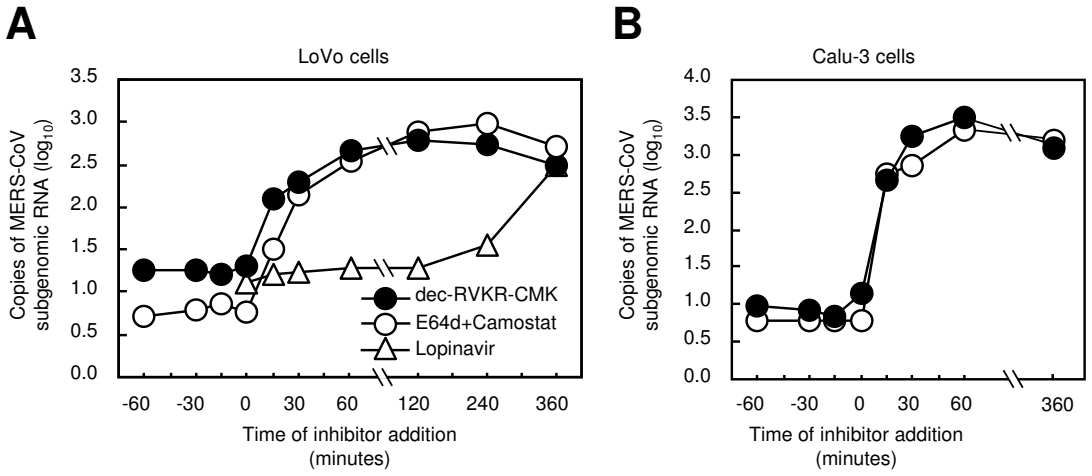

Figure 8